International Journal of Fatigue 202 (2026) 109148

Contents lists available at ScienceDirect

International Journal of Fatigue

journal homepage: www.elsevier.com/locate/ijfatigue

In-situ investigation and analytical modeling of crack initiation and propagation in Ti–6Al–4V under low-cycle fatigue conditions on microscale

Christopher M. Wuensch

Institute of Test and Simulation for Gas Turbines, German Aerospace Center, Forschungsallee 1, Augsburg, 86159, Germany

ARTICLE INFO

Keywords:
Ti–6Al–4V
In-situ investigation
Low-cycle fatigue
Hysteresis
Stage I crack propagation

ABSTRACT

Ti alloys such as Ti–6Al–4V belong to a group of materials that show tremendous potential in aircraft engine construction due to their mechanical properties and corrosion resistance. However, not only the knowledge of the material properties are relevant, but also a comprehensive understanding of the damage mechanisms that occur. One of the most relevant types of damage mechanisms is caused by the cyclic loading, as this accounts for more than 70% of the economically relevant damages, not only in the construction and operation of gas turbines. The objective of this study is he characterization of the crack growth behavior under low-cycle fatigue conditions on a phenomenological and mathematical-analytical level. In-situ LCF fatigue measurements revealed that favorable crack initiation due to slip band formation and propagation sites are located within β phases and at grain boundaries in Ti–6Al–4V. Crack closure and merging effects resulted in single but critical crack that lead to failure. In addition, the energetical investigation with elasto-plastic strain response showed a continuous increase in absorbed energy as consequence to formation of crack surfaces. The determination of crack growth rates completed the analytical investigation and enabled a full size modeling revealing advantages and potential of optimization of existing model.

1. Introduction

An essential step towards reducing the CO_2 footprint in aviation is the research and development of new aircraft engine technologies. One way to achieve this is the application of new and innovative materials with specific outstanding properties. Their use in gas turbines results in a significant weight reduction, which leads to fuel savings. Consequently, this lowers the operating costs and reduces the emission of pollutants. Nowadays, materials such as Ti–6Al–4V are used. This Ti alloy combines high strength with good corrosion resistance and temperature stability. The use of the Ti alloy in aviation led to the fact that the material properties could be understood and the knowledge could be consolidated. In contrast, the knowledge of the occurring damage mechanisms in Ti–6Al–4V still has potential for optimization. Particularly important is the investigation of damage process caused by cyclic fatigue [1,2].

Fatigue comprises the damage and failure of materials induced by cyclic applied loading conditions resulting in crack formation that leads to material failure. A fatigue crack results from localized plastic deformation during cyclic loading. The crack initiation site and crack formation process are typically determined by slip characteristics and properties of the material. In metals and metal alloys, irreversible dislocation movements of edge dislocations caused by cyclic loading leads to the formation of persistent slip bands. From crack initiation to fracture, fatigue cracks can be classified in two stages. Stage I cracks (or microstructurally short cracks) are those small enough that the material's microstructure influences the crack path. These cracks form on an active slip plane that is oriented 45° to the load axis. Microstructurally short cracks are smaller than 50 µm and are mainly analyzed by continuum mechanics approaches. The transition from short to long cracks are physically short cracks with lengths up to 100 µm. As these cracks grow larger, the crack paths develop in a more energetically favorable way often described as tension driven cracks [3]. The last type of cracks are larger cracks which are denoted as stage II cracks [4]. Such cracks are investigated by classical fracture mechanics models and show lengths larger than 100 µm [5].

Former studies showed, that the fatigue behavior of Ti alloys is very sensitive to the previous history of the material [6–9]. Besides grain orientation and the aspect of grain boundaries, the mean effective grain size is one of the parameters that affect the crack growth rate in $\alpha + \beta$ Ti alloys [10–14] at most. During crack initiation there is uncertainty about microstructure variations in Ti–6Al–4V [15,16]. One source of uncertainty is texture, having a strong influence on fatigue life. However, to clearly identify the effect of texture and its influence on microstructure is difficult, when changes in the microstructure occur simultaneously [17–19]. Conclusions of Peters et al. agree with

E-mail address: Christopher.Wuensch@dlr.de.

https://doi.org/10.1016/j.ijfatigue.2025.109148
Received 10 February 2025; Received in revised form 10 June 2025; Accepted 2 July 2025
Available online 30 July 2025

numerous studies and showed that crack initiation is closely related to thermomechanical treatment during manufacture of Ti alloys. Furthermore, Lucas et al. showed that the mean effective grain size has an influence, especially on the fatigue life of notched specimens [7,12].

Ivanova et al. investigated fatigue crack initiation sites in Ti–6Al–4V at low cycle fatigue [20]. For that, equiaxed cross-rolled and equiaxed forged Ti–6Al–4V alloys were investigated. They concluded, that for the equiaxed forged fatigue specimen first crack formation was detected at an α-β grain boundary. These cracks were smaller than 10 µm. However, after 9000 elapsed cycles slip band formation occurred in a neighboring α grain. After nearly 12000 elapsed cycles the crack propagated along slip bands. After nearly 24000 elapsed cycles the specimen fractured [21]. For the equiaxed cross-rolled Ti alloy, the crack formed within an α phase. After 15000 elapsed cycles, the crack propagated into the next α grain but circumvented the intermediate β phase. The results of this study showed that the α phase and α-β grain boundaries are preferred sites for crack initiation. Furthermore, it is claimed that crack initiation is controlled by cleavage fracture. This conclusion relates to the higher susceptibility of α phase fracture than β phase [21].

Considerations about microstructural processes lead to the conclusion that a modification of the Paris law is required to obtain proper analytical fatigue crack growth description [22]. Jones et al. investigated mathematical crack growth representation in Ti–6Al–4V [23]. Based on previous studies of Ritchie et al. that crack shielding effects and drop of the fatigue threshold have to be considered [24]. Investigations of Jones et al. are fundamental for the mathematical model for short and long crack growth described by the Hartman–Schijve equation [25]. For mill annealed Ti–6Al–4V, tests were performed at a stress ratio of R = 0.1, 0.4, 0.7 and 0.8. ΔK_{thr} and A were chosen to fit the measured crack growth rate as a function of ΔK. Based on the Hartman–Schijve equation Jones et al. derived the following crack propagation equation (Eq. (1)), where a is crack length, N the number of elapsed cycles and C and m material parameters [26].

$$\frac{da}{dN} = C\left(\frac{\Delta K - \Delta K_{thr}}{\sqrt{1-\frac{K_{max}}{A}}}\right)^{m} \tag{1}$$

In order to build up a comprehensive understanding of these processes an integral approach is chosen which combines both phenomenological investigation and numerical methods in order to better understand the physical phenomena in the material that lead to fracture in Ti–6Al–4V [27,28]. The phenomenological investigation is based on experiments and qualitatively characterizes the crack growth behavior from the initial state until material failure [29]. The numerical methods, based on the experimentally acquired data, are mainly concerned with the investigation of hysteresis data derived from fatigue and modeling of the crack growth behavior [30–32]. The objective of this study is the in-situ characterization of crack initiation and propagation in Ti–6Al–4V under low-cycle fatigue conditions on microscale. In contrast to the discussed studies, an uniaxial in-situ stage was used, allowing simultaneous investigation of crack growth under cyclic loading using a scanning electron microscope. The focus was the determination of the damage mechanism and the development of the crack path up to failure under the influence of the material's microstructure. Therefore, the chemical composition and microstructure of the tested Ti–6Al–4V were analyzed first, followed by the determination of mechanical properties in a second step. Afterwards fatigue tests have been conducted. The results ultimately feed into the crack propagation modeling. From the experimental perspective, the boundary conditions of the tests in the study were selected to correspond to the low-cycle fatigue since this represent the actual loading conditions of components in aircraft engines made out of Ti–6Al–4V.

Table 1
Chemical composition (wt.-%) of tested Ti–6Al–4V.

Ti	Al	V	Fe	C	N	O
77 ± 2	6 ± 1	4 ± 1	1 ± 0	9 ± 1	1 ± 1	1 ± 0

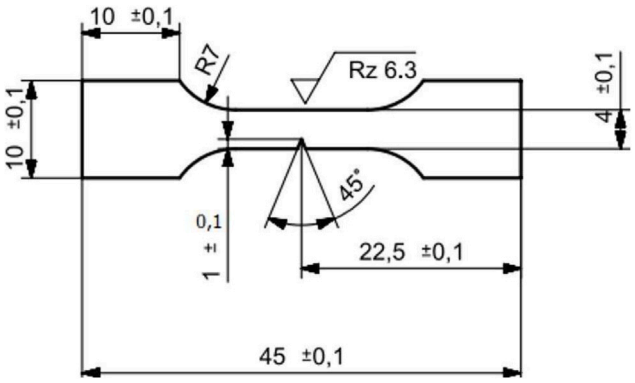

Fig. 1. Flat fatigue test specimen size manufactured from the alloy Ti–6Al–4V.

2. Materials and methods

2.1. Chemical composition and microstructural characterization

The material investigated in this study was annealed Ti–6Al–4V ($\alpha+\beta$). The chemical composition is given in Table 1. The semi-finished Ti–6Al–4V was hot rolled (1 × 1000 × 1000 mm), underwent a heat treatment of 1063 K for 60 minutes and then air cooled.

Flat test specimens were machined by electrical-discharge machining (EDM) from the semi-finished Ti–6Al–4V to the dimensions shown in Fig. 1, in accordance to ASTM-E8/E8M. The thickness of the flat test specimens is 1 mm. Especially on microscale, crack detection is challenging because large magnifications enable only a small monitoring area. Therefore, those flat specimens that were designated for fatigue experiments were notched additionally to obtain a region where crack initiation is favored. The notch is oriented perpendicular to the rolling direction and has an opening angle of 45° and a depth of 1 mm. This notch geometry result in a stress concentration factor of 2.2.

Afterwards, satisfactory grinding and polishing were carried out to remove the altered surface layer and visualize the material's microstructure. In order to keep the influence of polishing conditions on the crack initiation mechanisms as low as possible, polishing was repeated three times with ever-decreasing grain size emulsions. The emulsions were a solution of polycrystalline suspension and a water–ethanol detergent with grain sizes of 9, 3 and 0.1µm.

The bimodal microstructure was observed with an environmental scanning electron microscope (ESEM) as shown in Fig. 2. The microstructural characterization then proceeds in two steps, beginning with phase determination by local energy dispersive X-ray spectroscopy (EDS) measurements and followed by grain size determination. The combination of the investigations on the chemical composition, the determination of grain sizes and being familiar with the manufacturing conditions allows the phases to be assigned in a way, so that the influence on crack initiation and crack propagation can be determined.

The heat treatment resulted in a microstructure composed primarily of globular grains separated by intergranular precipitates in between. Chemical compositions of the globular and intergranular grains are listed in Tables 2 and 3 as derived by EDS. In accordance with these results, the globular grains belong to the α phase while the intergranular grains belong to the β phase. The overall fraction of α grains is 77% with an average grain size of 26 µm. The average size of β grains is 10 µm.

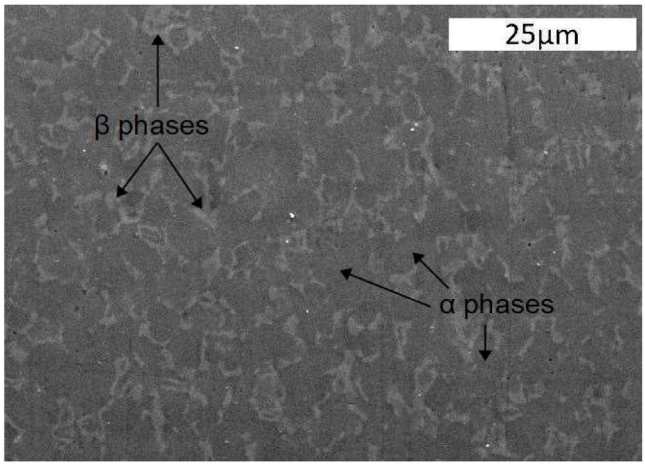

Fig. 2. Ti alloy's microstructure consists of primarily globular α grains with secondary intergranular β precipitates in between (Mag. 1500 x).

Table 2
Mean chemical composition (wt.-%) of intergranular α phases.

Ti	Al	V
79 ± 2	6 ± 0	2 ± 1

Table 3
Mean chemical composition (wt.-%) of intergranular β phases.

Ti	Al	V
75 ± 1	4 ± 0	7 ± 1

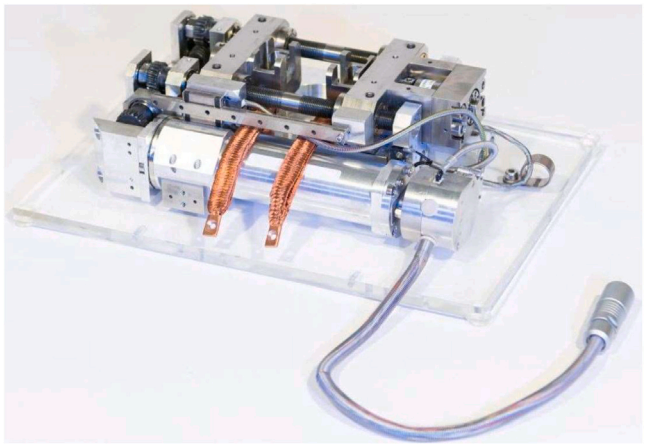

Fig. 3. Uniaxial in-situ stage for tensile and fatigue tests.

2.2. Tensile test setup and analysis

The tensile and fatigue tests were carried out in an uniaxial in-situ stage as shown in Fig. 3. Specifically, the in-situ stage provides loads up to 10 kN in quasistatic and dynamic-cyclic test scenarios. However, since only flat specimens can be examined, only stress ratios of ≥ 0 are possible. To clamp the specimen under pulling conditions small serrated wedges are used. Due its compact size (270 × 150 × 85 mm), the most notable advantage of this in-situ stage is the possibility of installation within an ESEM that enables in-situ measurements of failure mechanisms on micro level. Consequently, the examined crack initiation and stage I crack propagation can be correlated with the applied load and the specimen deformation simultaneously.

For a detailed design of LCF-fatigue experiments, the mechanical properties of the flat test specimens have to be known. For this purpose, three tensile tests with unnotched specimens the same size as in Fig. 1 were conducted. The specimen deformation was measured using an extensometer having an initial gauge length of 10 mm and in addition a linear encoder mounted on the side of the uniaxial in-situ stage. Result comparison allows conclusions to be drawn about the stage's stiffness. Tensile tests were carried out load-controlled and crosshead speed of 1 mm/min. Physical and mechanical properties of tested Ti–6Al–4V are listed in Table 4.

Table 4
Mean properties derived by tensile tests in uniaxial in-situ stage.

E (GPa)	$R_{p0.2}$ (MPa)	σ_{UTS} (MPa)
100.4 ± 1.3	953.2 ± 0.0	1037.5 ± 14.7

2.3. Fatigue tests and fractography

In total three notched specimens (Fig. 1) were tested in the uniaxial in-situ stage which was installed in the Thermofisher ESEM Quattro at room temperature in vacuum at a fatigue frequency of 0.06 Hz. This test setup enabled in-situ measurements of crack length during fatigue cycling. The maximum nominal stress for each specimen was 460 MPa with a stress ratio of 0. The stress state was chosen, so that considering the stress concentration factor of 2.2, plastic deformation in front of the notch tip was provided. Fatigue cycling was periodically interrupted in accordance to the development of crack propagation. As long as no crack initiation occurred, each 100 cycles the tests were interrupted in order to check, whether features of crack initiation have been formed. As soon as first features of slip band formation were observed, interruption was carried out every 20 elapsed cycles. This procedure was continued until stage II crack propagation became evident. From then on every 50–70 cycles the tests were interrupted until the specimens finally fractured. Since the expected damage mechanisms and stage I crack propagation influenced by the microstructure are in the order of a few micrometers, the investigation in the scanning electron microscope was carried out for resolution reasons. During each interruption a photo of the crack was taken with the ESEM and examined while applying the stress amplitude σ_a to the specimen. Therefore crack length was determined twice manually. First along a straight path from the notch tip to the crack tip which is indicated in the following as crack length. The second crack length measurement represents the actual crack path and is indicated as crack path length. In addition, the notch depth was taken into account for both measurements. Since the crack length measurements were conducted on the specimen's surface, it was assumed that the crack protrudes homogeneously into the specimen. Subsequent to failure, the fracture surface of the specimens was evaluated at first with an optical microscope to obtain a three-dimensional topography diagram and afterwards investigated with the ESEM to characterize the microstructural failure mechanism.

3. Results and discussion

3.1. Phenomenological description of fatigue behavior

3.1.1. Crack initiation and stage I propagation

While each fatigue specimen contained a notch, the notch depth of each specimen was determined individually and must not correspond to exactly 1 ± 0.1 mm in accordance to Fig. 1. Table 5 summarizes the observations of crack initiation for all tested specimens, where N_I represents the number of elapsed cycles when the crack was detected first.

In accordance with Fig. 4, the crack was detected after 739 elapsed load cycles for the first fatigue experiment. Starting point for this crack is the transition region between notch surface and specimen top surface. The combination of stress intensities resulting from the edge between notch and specimen top surface and the quality of

Table 5
Characteristics of fatigue behavior of tested Ti–6Al–4V specimens.

No.	N_i	No. of cracks initiated	Notch depth (μm)
01	739	1	740 ± 4
02	458	1	694 ± 5
03	491	1	694 ± 4

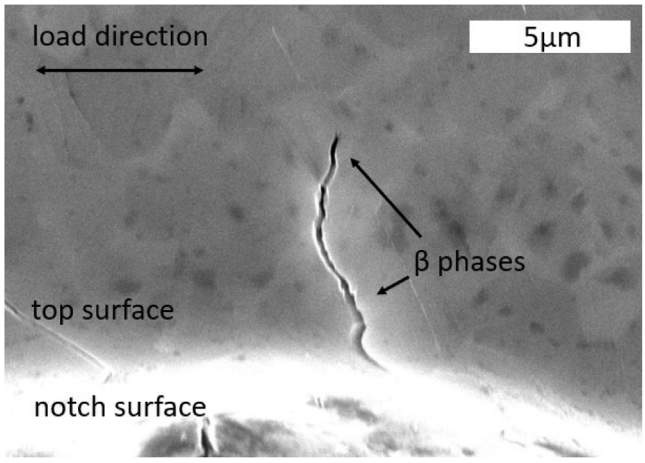

Fig. 4. Crack initiation site on the first fatigue specimen after 739 elapsed cycles (Mag. 6500 x).

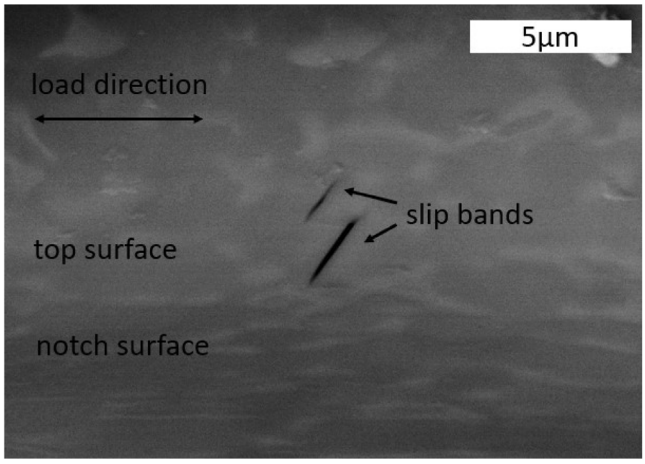

Fig. 5. Slip band formation in an angle of 55° to the load direction on the second fatigue specimen after 458 elapsed cycles (Mag. 6500 x).

the notch surface topography that promoted crack initiation in the transition region. In the initial stage of crack growth on the specimen's top surface, it propagated first through a β phase, extended along a α-β phase boundary before penetrating another β phase. Furthermore, the microstructurally short crack growth was dominated by strong changes of crack path directions, especially in the transition region. No appearance of slip band formation was observed for this specimen.

For the second specimen, the effects of slip band formation became evident after 458 elapsed cycles (Fig. 5). The crack initiated within a β phase located at the edge of the specimen's top surface. After 600 load cycles, another slip band formation in another β phase was observed parallel to the first slip band. Both slip bands were oriented in an angle of 55° ± 2° to the applied load direction.

For the third specimen, the crack was detected first after it proceeded to propagate through the notch surface and then on the top surface. Whether the crack formed on the bottom surface or in the notch

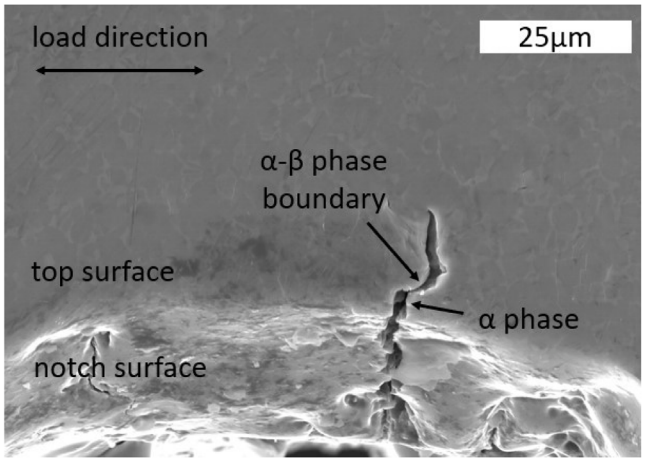

Fig. 6. Crack initiation site on the third fatigue specimen after 491 elapsed cycles (Mag. 6500 x).

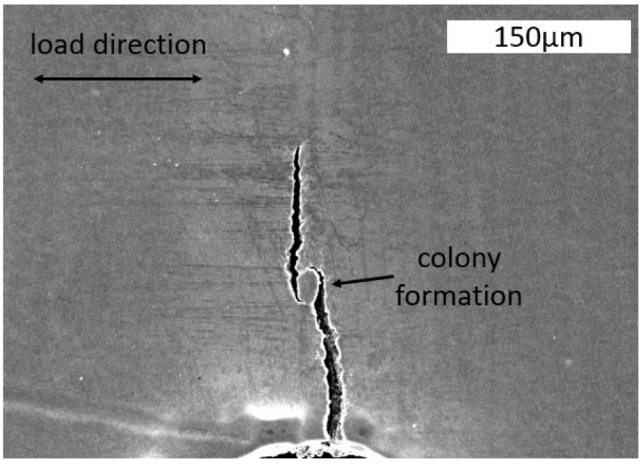

Fig. 7. Colony formation and stage II crack propagation after 2430 elapsed cycles for the first specimen (Mag. 250 x).

plane, remains unclear. When the crack reached the top surface, it penetrated through an α phase in load direction and along an α-β phase boundary. At the end of this interface, the crack started to orientate perpendicular to load direction after 491 load cycles (Fig. 6).

3.1.2. Multiple crack formation and stage II propagation

After 1020 load cycles, beside the monitored crack two other cracks were observed on the top of the surface of the first specimen. One of these two cracks developed in an α phase in front of the monitored crack tip while the other one formed on the left side of the main crack. Both showed stage I crack propagation behavior due to strong crack path direction deviations induced by the materials microstructure. After 1179 cycles the small crack in front of the crack tip and the monitored crack merged and continued propagation while two new cracks formed in two different β phases in front of the monitored crack. Both cracks merged with the monitored crack after 1487 elapsed cycles. At 1884 load cycles the monitored crack split and started to propagate in two different directions. One perpendicular to load direction while the other one parallel to load direction. After 2430 load cycles as shown in Fig. 7 material colony formation became evident and both cracks merged to one main crack, that started to propagate perpendicular to load direction. From that point on, the crack showed stage II crack propagation.

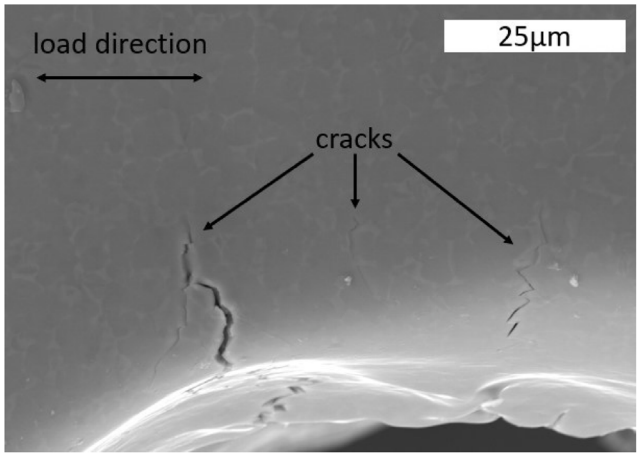

Fig. 8. Multi cracking on the specimen's notch edge and crack merging on the left side after 1702 elapsed cycles in the second test (Mag. 1500 x).

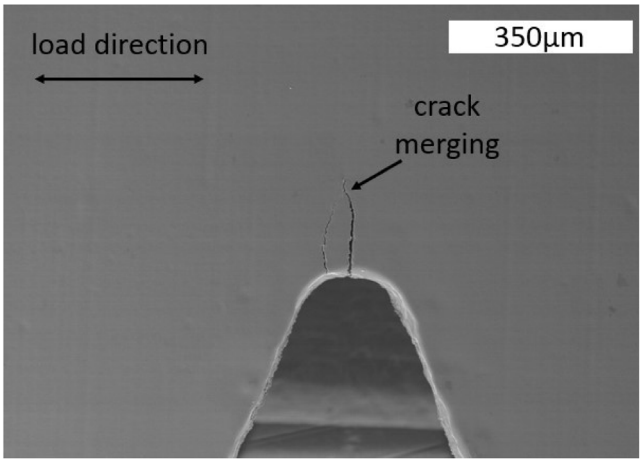

Fig. 9. Sudden crack growth of the right crack and crack tip merging after 3803 cycles in the second test(Mag. 100 x).

In comparison to the first specimen, multi crack formation for the second specimen became more significant. First multi cracking was observed after 1205 load cycles. Two cracks have formed left of the slip band formation shown in Fig. 5. While the slip band formation occurred out of the center of the notch tip, one crack formed at the notch tip center while the second one developed out of the notch tip center. For both cracks, there were no indications of slip band formation observable. After 1702 elapsed cycles, the crack originating from slip band propagated into the notch plane showing strong deviations in direction due to the material's microstructure. Additionally, the crack on the left-hand side merged with another crack that approached from the notch plane.

Fig. 8 shows the second specimen after 2352 elapsed cycles. The crack on the right-hand side propagated mainly through β phases. The crack in the center indicated by an arrow stopped and almost vanished, while the crack on the left-hand side seems to be the dominating crack penetrating mostly β phases. After 3803 cycles the crack originating from slip band formation interrupted propagation and merged with the former dominating crack as shown in Fig. 9. Furthermore the physically short crack turned into a stage II crack and is not influenced by material's microstructure.

The early crack growth behavior for the third specimen was similar for the first specimen without any multi crack formation. After 521 elapsed cycles two smaller cracks formed and merged afterwards

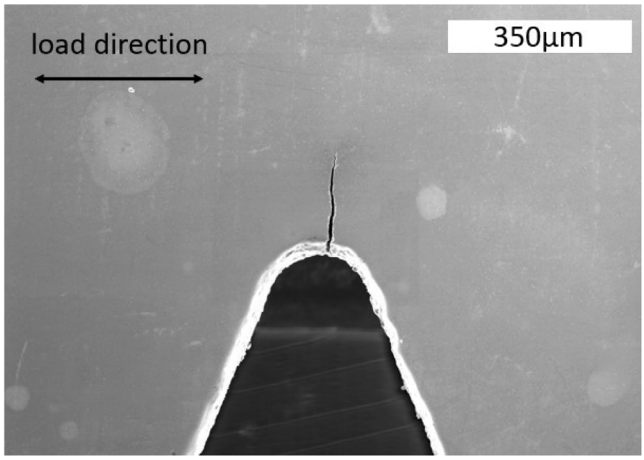

Fig. 10. Stage II crack propagation for the third specimen after 1091 cycles (Mag. 100 x).

Table 6
Characteristics of fracture behavior initiated by fatigue loading of tested Ti–6Al–4V specimens.

No.	N_f	Final crack length (µm)
01	2784	1833 ± 4
02	4239	1873 ± 5
03	1659	1814 ± 4

with the monitored crack. Except for one direction change, the crack penetrated α and β phases without being affected by them. After 1091 cycles, the monitored crack showed stage II behavior (Fig. 10).

3.1.3. Mixed mode loading and fracture

Unstable and sudden crack growth resulted in fast crack propagation that led to fracture of the specimens. For this Table 6 summarizes the observations, while N_f represents the elapsed cycles until fracture.

For the first specimen, mixed mode loading effects became evident after 2731 cycles that result in crack path deflection towards applied load direction. This effect indicated first signs of failure due to inhomogeneous load distribution applied to the intact cross section of the specimen. After 2784 elapsed cycles the specimen suddenly fractured. The second and third specimen behave similar as the first specimen considering fracture. Crack path deflection for the second specimen was significant observable after 4204 cycles (Fig. 11) while for the third specimen after 1640 cycles. The second specimen fractured after 4239, the third specimen after 1659 elapsed cycles.

3.1.4. Fractography

Fractography was performed for all fatigue specimens using an optical microscope and ESEM. Exemplary the fractograph of the fracture surface of second test is shown below (Fig. 12). The figure shows both halves of the tested specimen on top of each other.

Each cross-sectional surface can be split into three areas — the notch surface, the fracture surface induced by cyclic loading and the residual fracture surface. The planar fracture surfaces resulting from fatigue are characterized by metallic shiny and pointed surfaces. In addition, cracks that result from the early stages of fatigue starting at the notches intrude almost 400 µm into the bulk material can be observed. As indicated in Fig. 13, striation formation was investigated on microscale.

Considering the residual fracture surfaces in Fig. 13 a combination of intergranular brittle fracture and ductile fracture had developed. The reason for this is that there is no plastic deformation in the fracture zone

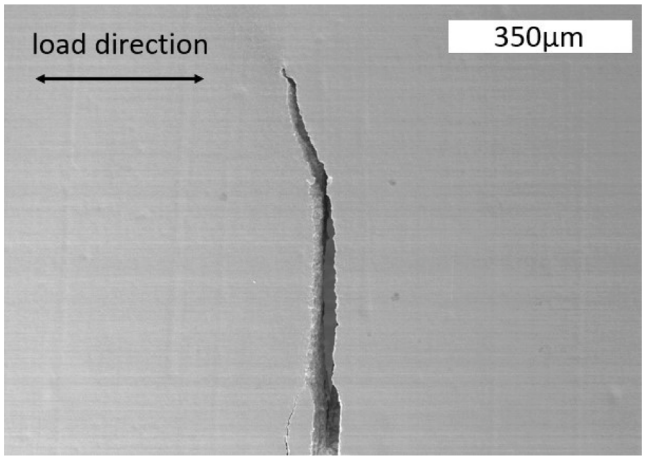

Fig. 11. Crack deflection after 4236 elapsed cycles investigated in the second test (Mag. 100 x).

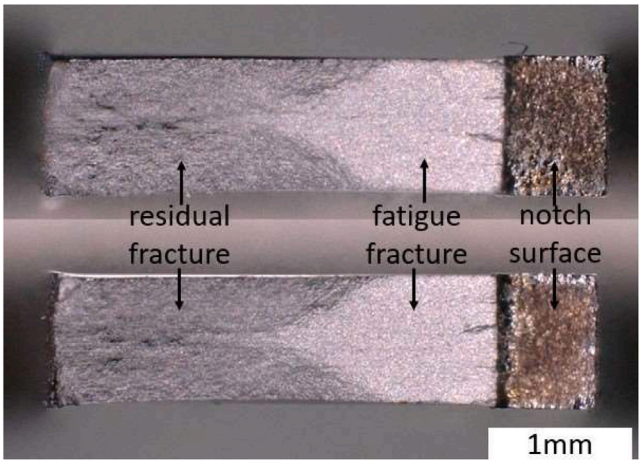

Fig. 12. Fracture surfaces of the second fatigue specimen (Mag. 50 x).

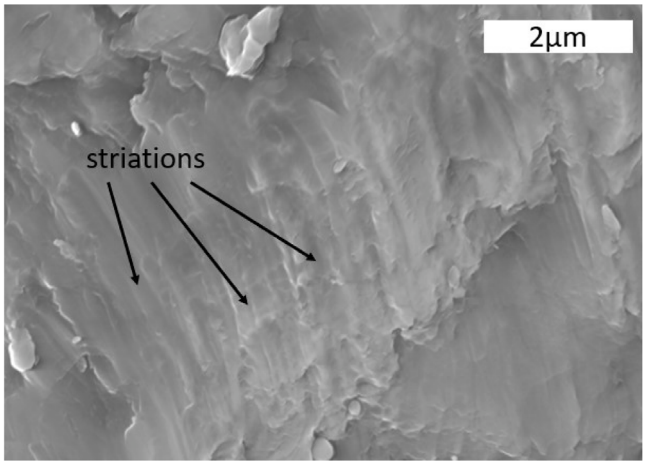

Fig. 13. Microstructural striations on the fatigue fracture surface of the second specimen (Mag. 15000 x).

on macroscopic level but on microscopic level slip phenomena and void development were observable (Fig. 14).

Further reason for proportional ductile fracture is that the developed residual fracture surfaces for all specimens are inclined (Fig. 15).

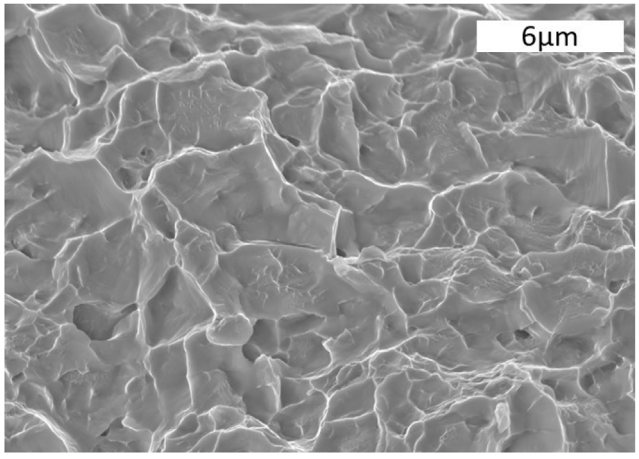

Fig. 14. Void development on the residual fracture surface of the second specimen (Mag. 15000 x).

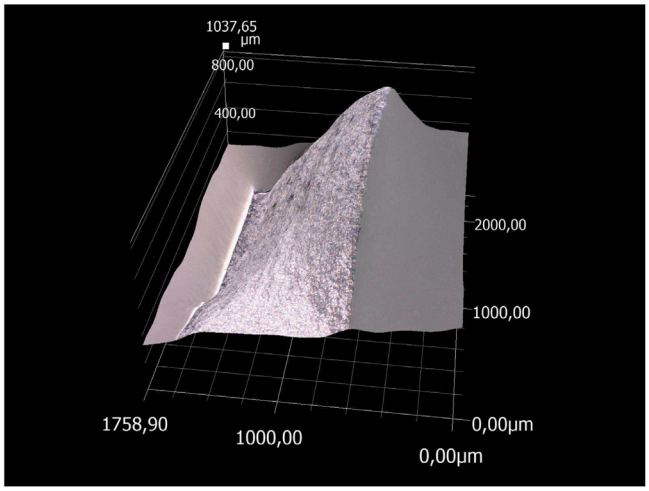

Fig. 15. 3-dim. view of the top side inclined residual fracture surface of the second specimen (Mag. 150 x).

This phenomenon occurs, if the actual shear stress exceed the critical shear stress in accordance to Schmid's law.

3.2. Crack growth analysis and modeling

3.2.1. Characteristics of crack growth

The investigation of crack growth behavior in dependent on the number of cycles enables first conclusions about crack growth rates. For this, crack lengths were measured optically on the top surface of the specimens as described in 2.3. The results of all experiments are shown in Fig. 16. In accordance with Fig. 16, the crack growth characteristics are given in Table 7.

In the beginning of each experiment, crack initiation and slow crack growth is dominating. Consequently, the measured crack lengths are small. The developed stage I cracks are affected by microstructure, load ratio and environmental effects. At mid-range, the influence of microstructure, environment and load ratio on crack propagation decreases while energy efficient crack growth behavior becomes evident. As a result, the crack growth rates increase. In the end, unstable and rapid crack growth dominates. This results in high crack growth rates and fracture. As stated in 3.1, for the first specimen (red curve in Fig. 16) the crack was detected first at 739 load cycles. After 2430 elapsed cycles, the crack started to turn into a stage II crack and after 2784

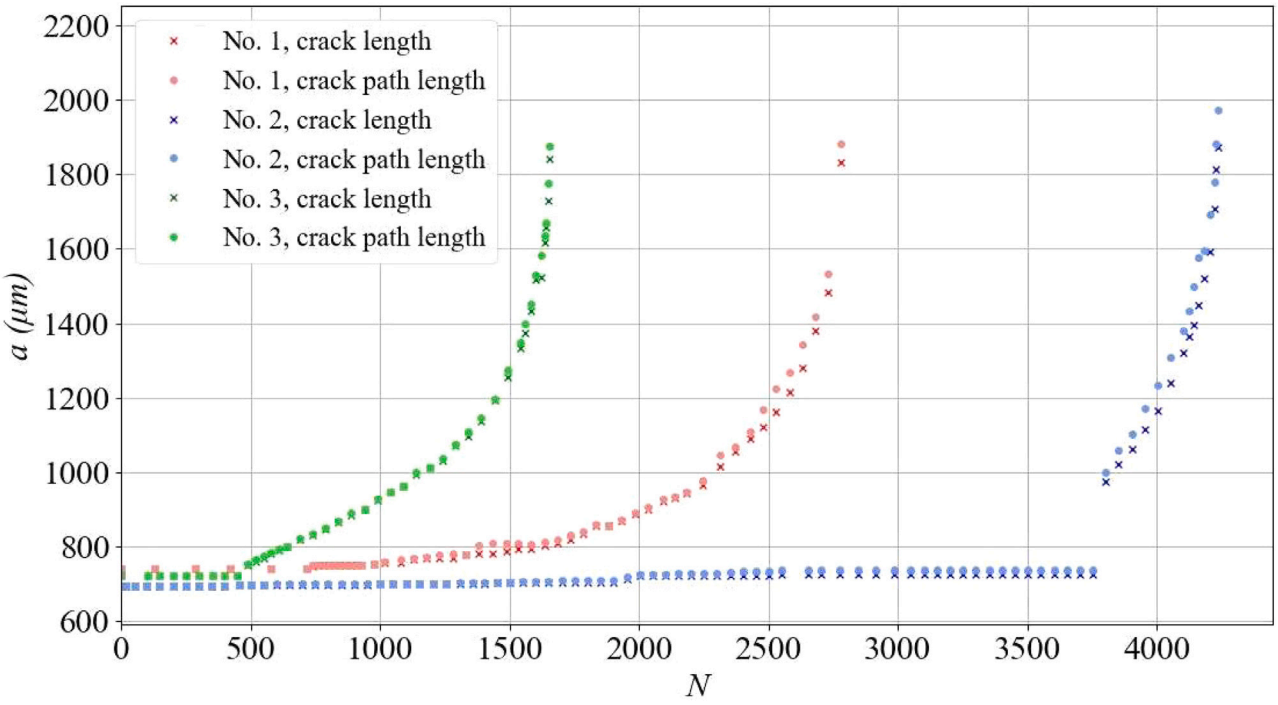

Fig. 16. Results of crack lengths and crack path lengths.

Table 7
Characteristics of fatigue behavior of tested Ti–6Al–4V specimens.

No.	N_I	N_f	N_I/N_f (%)	Max. crack length (μm)	Max. crack path length (μm)
01	739	2784	26.5	1833 ± 4	1881 ± 4
02	458	4239	10.8	1873 ± 5	1972 ± 5
03	491	1659	29.6	1814 ± 4	1877 ± 5

cycles the specimen fractured. The blue curve in Fig. 16 illustrates the crack propagation of test No. 2. Slip band formation and crack initiation was detected after 458 cycles as described in 3.1.1. After 1205 load cycles first multi cracking was detected. Two other cracks have formed close to the monitored crack. Initially, further cycling did not lead to further crack growth, but after 3803 cycles a sudden crack growth began. The existing cracks that resulted from multi cracking merged into a single main crack. The sudden crack growth resulted from the release of stored energy introduced into the material by the cyclic loading. At 4239 cycles the specimen fractured. In addition, the sudden crack growth led to further stress relief in the area in front of the crack tip. The data for the third specimen is plotted as green curve in Fig. 16. The crack, where crack initiation location remains unclear, was detected first at cycle 491. After 1091 cycles, the microstructurally short crack began to turn into a stage II crack. Ultimate fracture occurred after 1659 cycles.

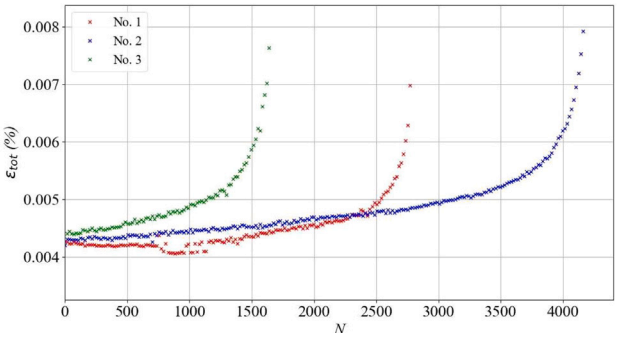

Fig. 17. Elasto-plastic strain response for all three specimens.

3.2.2. Fatigue hysteresis investigation

Hysteresis loops evolve in time. An uncommon but valid way to investigate mechanical cyclic response is the execution of load-controlled fatigue experiments as performed in this study. In this case the investigated parameter is total strain based on elapsed cycles which are shown in detail in Fig. 17.

According with Fig. 17, all specimens show an increase in total strain during fatigue loading. For all further considerations, reference is made to the nominal strain, which was determined using an extensometer attached to the undersides of the flat fatigue specimens. Further observations of the strain response reveal an incremental increase in total strain for almost two-thirds of the fatigue life of each specimen. Comparing the data in Table 7 with the results in Fig. 17, effects such as crack initiation and early crack growth cannot be clearly identified or separated from each other in terms of the number of cycles. The last third of fatigue life is dominated by accelerated increase in total strain. This is mainly dominated by unstable crack growth and crack path deflection due to mixed-mode loading conditions. The strain energy per elapsed cycle that is released during fatigue is illustrated in Fig. 18.

The strain energy per cycle is calculated based on the elasto-plastic strain response in combination with the applied load [33]. Therefore, the strain energy has been derived from the integration of each single hysteresis loop. Due to the fact that only plastic deformation creates an enveloped area in the cyclic stress–strain diagram, the strain energy

Table 8
Characteristics of fatigue behavior of tested Ti–6Al–4V specimens.

No.	Min. plastic strain energy (mJ/mm^3)	Max. plastic strain energy (mJ/mm^3)	Tot. plastic strain energy (J/mm^3)
01	0.0011 ± 0.0007	0.270 ± 0.004	$182.07*10^3$
02	0.0001 ± 0.0001	0.426 ± 0.017	$106.28*10^3$
03	0.0037 ± 0.0007	0.209 ± 0.008	$51.98*10^3$

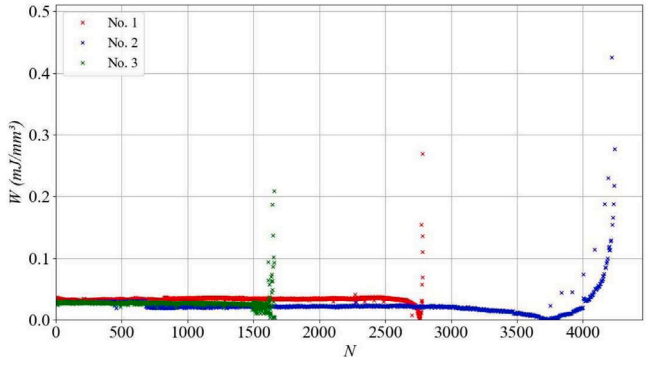

Fig. 18. Strain energy released during fatigue.

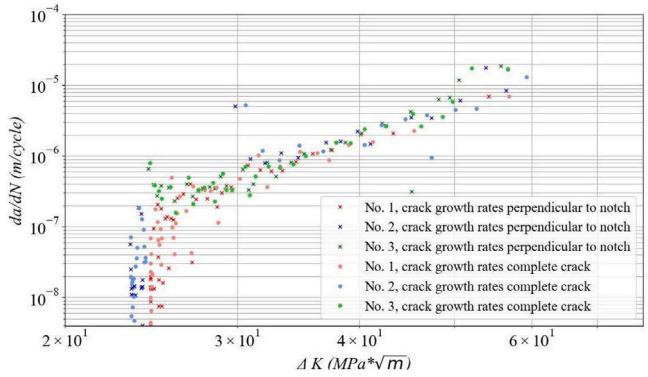

Fig. 19. Crack growth curves for all tested specimen according to Jones et al..

corresponds to the plastic strain. This is in accordance with the aspect that cyclic damage can be traced back to a series of occurring plastic deformation. However, the data show that the strain energy per cycle stays constant until the final stages of fatigue life are reached. At this point, the strain energy per cycle W decreases almost to 0 mJ/mm^3. The area of the individual hysteresis curves is small in this regime. This corresponds to almost no plastic deformation of the specimen. Afterwards the strain energy per cycle rapidly increases due to final fracture. From this data, the total strain energy that is released can be calculated by the number of cycles to fracture and the strain energy per cycle (Table 8).

3.2.3. Crack propagation modeling

Near-threshold and stage II fatigue crack growth data measured at R=0 condition for all specimens are presented in Fig. 19. in relation to the model proposed by Jones et al. (Eq. (1)), the material parameters C, m and A are optimized so that it represents the data sets at its best. ΔK_{max}, ΔK_{thr} and C, m and A values defined from these tests are listed in Table 9.

Comparing the data in accordance with the crack growth rate, the largest difference can be observed in the final fatigue test. This is attributed to the initial crack growth stop at the beginning and the subsequent abrupt crack growth in the transition between short crack and long crack. However, the crack growth rates close to the threshold range are between $4*10^{-8}$ m/cycle to $5*10^{-6}$ m/cycle. These values can be assigned to both intergranular and transgranular crack propagation phenomena as described in 3.1. The stable crack growth region in Fig. 19, defined by crack propagation rates larger than $5*10^{-6}$ m/cycle is dominated by stage II crack propagation phenomena mainly showing multi crack development and mixed mode loading conditions. Unstable crack growth is not addressed in this study.

4. Conclusion

In this study, the main objective is the detailed full-size characterization of the fatigue behavior of Ti–6Al–4V using scale-resolving in-situ measurement techniques. The results show the importance of a detailed description of occurring phenomena under cyclic loading in connection with the optimization of existing crack growth models and a comprehensive numerical investigation. The detailed results are as follows:

(1) In accordance with the previous literature, this study shows that crack initiation in Ti–6Al–4V is influenced by various aspects. In two out of three cases, the crack initiation took place within the notch, so sufficient detection was possible. Both cracks were monitored after they reached the top plane of the specimens. In one case, crack initiation caused by slip band formation in a β phase was detected. In the same experiment, the formation of several cracks could be observed. However, crack closure and crack merging effects lead to a single macro crack that results in fracture.
(2) Stage II crack propagation and macro crack behavior was characterized by the energetically favorable orientation of the cracks as well as the formation of small microcracks in front of the crack tip. Due to the high loads during single stage loading in combination with the crack length, mixed mode loading was detected before the specimens fractured. This results in a deviation of the crack path from the most energetically favorable direction.
(3) Investigation of fracture surfaces was split into two parts, the first part discusses the fracture surface caused by fatigue fracture and the second part covers the investigation of the fracture surface during material failure. The first fracture surface was characterized by the formation of striation embedded in rough shiny surface. The second, strong inclined fracture surface represents a combination of ductile and brittle fracture.
(4) Accurate in-situ measurements of crack growth in accordance with elapsed cycles demonstrate that crack initiation occurs in the first third of fatigue life. The stress–strain response of single stage loading under LCF conditions lead to the formation of hysteresis. Analysis then shows continuous dissipation of energy and an increase in total strain during cyclic loading. This indicates that the investigation of stiffness behavior as well as the consideration of the specimen elongation is an adequate method to draw conclusions on the crack growth behavior in Ti–6Al–4V.
(5) Crack propagation modeling according to the equation suggested by Jones et al. confirms that the equation's structure is sufficient to describe stable crack growth. However, the modeling reveals that an optimization of the material parameters C, m and A must be considered. This study shows that microstructurally short and large cracks can both be modeled by the equation of Jones et al. even for small specimens outside standard sizes.

Table 9
Material parameters according to Jones et al. modeling.

No.	C_{Cl}	m_{Cl}	A_{Cl}	C_{Cpl}	m_{Cpl}	A_{Cpl}
01	$2.79*10^{-10}$	2.12	60	$2.79*10^{-10}$	2.12	58
02	$2.79*10^{-10}$	2.12	60	$2.79*10^{-10}$	2.12	65
03	$2.79*10^{-10}$	2.12	61	$2.79*10^{-10}$	2.12	68

5. Outlook

Considering the chosen in-situ method to monitor fatigue cracking behavior in Ti–6Al–4V, the results gained could be supplemented by further investigations. One example is electron backscattered diffraction in combination with the uniaxial in-situ stage, that enables measurement of interactions between grain orientation and phase boundaries and the development of microcracks [26]. In addition, the investigation of strain states surrounding the crack tip using digital image correlation contribute to an extensive description of micro cracking phenomena [34–36]. Also, the idea of fatigue testing close to conditions existing in a gas turbine, mainly high temperature and hot corrosion effects can be promising considering fatigue life characterization. This will require considerable effort in the use of measurement techniques. The existing mathematical models that describe crack propagation cover only a fraction of the existing modeling possibilities. Since each model focuses on individual aspects of fatigue behavior (i.e. stable crack growth or crack initiation), it is possible to use the data obtained to optimize current models in a way so that a comprehensive modeling is possible. This results in new findings complete the description of the crack growth behavior in Ti–6Al–4V. These enhancements in combination with the automation of the test procedure thus allow a profound and efficient investigation of the damage mechanisms present in Ti–6Al–4V and other materials.

Declaration of competing interest

The authors declare that they have no known competing financial interests or personal relationships that could have appeared to influence the work reported in this paper.

Acknowledgment

This work (No. ZF4688001DF9) was supported by Zentrale Innovationsprogramm Mittelstand (ZIM) from the Federal Ministry for Economic Affairs and Climate Action, Germany.

Data availability

Data will be made available on request.

References

[1] Udomphol T. Titanium and its alloys. Suranaree Univ Technol 2007.
[2] Dungey C, Bowen P. The effect of combined cycle fatigue upon the fatigue performance of TI-6Al-4V fan blade material. J Mater Process Technol 2004;153–154:374–9.
[3] Chan KS. Roles of microstructure in fatigue crack initiation. Int J Fatigue 2010;32:1428–47.
[4] Miller KJ. The behavior of short fatigue cracks and their initiation part II - general summary. Fatigue Fract Engng Mater Struct 1987;10:93–113.
[5] Künkler B, Düber O, Köster P, Krupp U, Fritzen C, Christ H. Modelling of short crack propagation - Transition from stage I to stage II. Eng Fract Mech 2007;75:715–25.
[6] Mulay RP, Moore JA, Florando JN, Barton NR, Kumar M. Microstructure and mechanical properties of Ti-6Al-4V: Mill-annealed versus direct metal laser melted alloys. Mater Sci Eng A 2016;666:43–7.
[7] M. Peters A Gysler, Lüetjering G. Influence of Microstructure on the Fatigue Behavior of Ti-6Al-4V. In: Titanium '80: Scinece and Technology, vol. 3, 1980, p. 1777–86.
[8] Stubbington AW, Bowen AW. The Effect of (α)+(β) Working on the Fatigue and Tensile Propertiesof Ti-6Al-4V Bars. Titan Sci Technol 1973;2097–108.
[9] Caton MJ, John R, Porter WJ, Burba ME. Stress ratio effects on small fatigue crack growth in Ti-6Al-4V. Int J Fatigue 2012;38:36–45.
[10] Zhao YQ, Xin SW, Zeng WD. Effect of major alloying elements on microstructure and mechanical properties of a highly β stabilized titanium alloy. J Alloy Compunds 2009;481:190–4.
[11] Lu J, Ge P, Zhao Y. Recent Development of Effect Mechanism of Alloying Elements in Titanium Alloy Design. Rare Met Mater Eng 2014;43:775–9.
[12] Lucas JJ. Improvements in the Fatigue Strength of Ti-6Al-4V Forgings. J Am Helicopter Soc 1971;2081–95.
[13] Hall J, Pierce C, Ruckle D, Sprague R. Property-Microstructure relationships in the Ti-6Al-2Sn-4Zr-6Mo-Alloy. Mater Sci Eng 1972;9:197–210.
[14] Yoder G, Coley L, Crooker T. A Comparison of Microstructural Effects on Fatigue-Crack Initiation and Propagation in Ti-6Al-4V. 1982, p. 132–6.
[15] Eylon D, Pierce CM. Effect of Microstructure on Notch Fatigue Properties of Ti-6Al-4V. Met Trans A 1976;7A:111–21.
[16] Hu Y, Floer W, Krupp U, Christ H. Microstructurally short fatigue crack initiation and growth in Ti-6.8Mo-4.5Fe-1.5Al. Mater Scinece Eng 2000;A278:170–80.
[17] Yoder G, Cooley L, Crooker T. Observations on the Generality of the Grain-Size Effect on Fatigue Crack Growth in (α)+(β) Titanium Alloys. 1980, p. 1865–73.
[18] Sadananda K, Vasudevan AK. Fatigue crack growth behavior of titanium alloys. Int J Fatigue 2005;27:1255–66.
[19] Sinha V, Mercer C, Soboyejo WO. An investigation of short and long fatigue crack growth behavior of Ti-6Al-4V. Mater Sci Eng 2000;A287:30–42.
[20] Invanova S, Biederman R, Jr. R Sisson. Investigation of Fatigue Crack Initiation in Ti-6Al-4V During Tensile-Tensile Fatigue. J Mater Eng Perform 2002;11:226–31.
[21] Askeland DR. Materialwissenschaften grundlagen-übungen-lösungen, first ed.. Spektrum Akademischer Verlag; 1996, p. 383–90.
[22] Ciavarella NPugnoand M, Cornetti P, Carpinteri A. A generalized Paris' law for fatigue crack growth. J Mechancs Phys Solids 2006;54:1333–49.
[23] Jones R, Michopoulos JG, Iliopoulos AP, Singh Raman RK, Phan N, Nguyen T. Representing crack growth in additively manufactured Ti-6Al-4V. Int J Fatigue 2018;116:610–22.
[24] Ritchie R, Yu W, Blom A, Holm D. An analysis of crack tip shielding in aluminium alloy 2124: A comparison of large, small through-crack and surface fatigue cracks. Fatigue Fract Eng Mater Struct 1987;10:343–63.
[25] Forman RG, Shivakumar V, Cardinal JW, Williams LC, McKeighan PC. Fatigue Crack Growth Database for Damage Tolerance Analysis. 2005, FAA.
[26] Krupp U, Düber O, Christ B, Künkler HJ, Schick A, Fritzen C. Application of the EBSD technique to describe the initiation and growth behavior of microstructurally short fatigue cracks in a duplex steel. J Microsc 2004;213:313–20.
[27] Chapetti MD. Fatigue propagation threshold of short cracks under constant amplitude loading. Interational J Fatigue 2003;25:1319–26.
[28] Zhang S, Zeng W, Zhao Q, Ge L, Zhang M. In situ SEM study of tensile deformation of a near-β titanium alloy. Mater Sci Eng A 2017;708:574–81.
[29] Oguma H, Nakamura T. Fatigue crack propagation properties of Ti-6Al-4V in vacuum environments. Int J Fatigue 2013;50:89–93.
[30] Wang K, Wang F, Cui W, Hayat T, Ahmad B. Prediction of short fatigue crack growth of Ti-6Al-4V. Fatigue Fract Eng Mater Struct 2014;37:1075–86.
[31] Jiang Y, Feng M. Modeling of Fatigue Crack Propagation. J Eng Mater Technol 2004;77:77–86.
[32] Chapetti M. Application of a threshold curve model to high-cycle fatigue behavior of small cracks induced by foreign-object damage in Ti-6Al-4V. Int J Fatigue 2005;27:493–501.
[33] Roy S, Goyal S, Sandhya R, Ray S. Analysis of Hysteresis Loops of 316L(N) Stainless Steel under Low Cycle Fatigue Conditions. Procedia Eng 2013;55:165–70.
[34] Lorenzino P, Beretta G, Navarro A. Application of Digital image Correlation (DIC) in resonance machines for measuring fatigue crack growth. Frat Ed IntegritÀ Strutt 2014;30:369–74.
[35] Bhavikatti S, Bhat M, Murthy C. Fatigue Crack Growth Monitoring in Ti-6Al-4V Alloy Using Acoustic Emission Tecnique and Digital Image Correlation. 2011.
[36] Vasco-Olmo J, Diaz F, Antunes F, James M. Characterization of fatigue crack growth using digital image correlation measurements ofplastic CTOD. Theor Appl Fract Mech 2019;101:332–41.